



**HAL**  
open science

## Experimental approach for microscale mechanical characterization of polymeric structured materials obtained by additive manufacturing

Joseph Marae Djouda, Mohamed Ali Bouaziz, Marouene Zouaoui, Matthieu Rambaudon, Julien Gardan, Naman Recho, Jérôme Crépin

### ► To cite this version:

Joseph Marae Djouda, Mohamed Ali Bouaziz, Marouene Zouaoui, Matthieu Rambaudon, Julien Gardan, et al.. Experimental approach for microscale mechanical characterization of polymeric structured materials obtained by additive manufacturing. *Polymer Testing*, 2020, 89, pp.106634. 10.1016/j.polymertesting.2020.106634 . hal-03050652

**HAL Id: hal-03050652**

**<https://uca.hal.science/hal-03050652>**

Submitted on 22 Aug 2022

**HAL** is a multi-disciplinary open access archive for the deposit and dissemination of scientific research documents, whether they are published or not. The documents may come from teaching and research institutions in France or abroad, or from public or private research centers.

L'archive ouverte pluridisciplinaire **HAL**, est destinée au dépôt et à la diffusion de documents scientifiques de niveau recherche, publiés ou non, émanant des établissements d'enseignement et de recherche français ou étrangers, des laboratoires publics ou privés.



Distributed under a Creative Commons Attribution 4.0 International License

## **Experimental approach for microscale mechanical characterization of polymeric structured materials obtained by additive manufacturing.**

Joseph MARAE DJOUDA<sup>1,2</sup>, Mohamed Ali BOUAZIZ<sup>1</sup>, Marouene ZOUAOUI<sup>1,3</sup>, Matthieu RAMBAUDON<sup>2</sup>, Julien GARDAN<sup>1,3</sup>, Naman RECHO<sup>2,4</sup>, Jérôme CRÉPIN<sup>2</sup>

<sup>1</sup>*ERMESS, EPF-Engineering school, 3 bis Rue Lakanal, 92330 Sceaux, France*

<sup>2</sup>*Centre des Matériaux, MINES ParisTech, CNRS UMR 7633, BP 87, 91003, Évry, France*

<sup>3</sup>*Institut Charles Delaunay, LASMIS, UTT, UMR CNRS 6281, 12 rue Marie Curie, 10010 Troyes, France*

<sup>4</sup>*Université Clermont Auvergne, Institute Pascal CNRS-UMR 6602, PB 10448, 63000 Clermont-Ferrand, France*

### **Abstract:**

In this paper, an original experimental method is developed for local strain characterization at the surface of additively manufactured polymeric materials. The process used herein is material extrusion. This experimental method is based on the use of microscopic speckle pattern deposited at the surface of micro single edge notched specimen ( $\mu$ \_SENT) made of acrylonitrile butadiene styrene (ABS). Two configurations of filament orientation were used for the specimen manufacturing. Images of the  $\mu$ \_SENT specimen surface were recorded during in-situ tensile test. The quantitative analysis of images was made by digital image correlation (DIC). The evolutions of the local strain heterogeneities and the crack tip are evidenced on the kinematic fields. It is shown that the crack propagates in the low resistance path which is the interface area between filaments. It is also evidenced that the intersection of perpendicular filaments in two adjacent layers blocks crack growth. The local strain evolutions at the surface of the specimen are compared to the macroscopic response of the material. The method developed herein allows the determination of the materials mechanical properties. The identification of the crack tip location using digital image correlation (DIC) and J-integral calculation lead to plot the J-R curve. The J-R curves comparison of the two specimen configurations shows that the fracture toughness is directly related to the material structure.

### **Introduction**

Additive manufacturing (AM) is used and is the subject of several researches and developments in many areas such as the aerospace, medical and automotive industries [1]. Prototyping still the most common AM use case [2], but in recent years, the production of functional and end-use parts by 3D printing is growing. There is a real interest from industries to bring AM to level of one of the main production engineering route [3]. However, in order to use this technology as common way to manufacture functional objects, there still two main issues to address: material and metrology to achieve the functionality in predictive and reproductive ways [3]. Therefore, the major challenge of AM research works was to improve the mechanical properties and object quality using various experimental techniques and concepts [4–6].

The kinematic field measurements, such as displacements or strains, are paramount to good material engineering and a better introduction in structural applications. For 3D printed material, especially obtained by extrusion material process where the molten filaments are

welded, it is important to characterize how the local heterogeneities of the structure affect the global mechanical properties. Local scale characterization methods are influenced by the material nature (polymeric, metallic or ceramic). In fact, most of the methods of local mechanical characterization are based on the use of random or periodic gratings [7–13]. Depending to the material nature, different technique of grating deposition or imposition can be used to improve the surface state. The deposition and annealing of metal thin layer is naturally used for metallic specimen [9]. This technique for example is limited for polymeric specimens because of the annealing temperature. Moreover, others routes using chemical solutions (ethanol, ketone, methyl isobutyl ketone and others) are not adapted for polymeric materials. The lithographic technique and chemical surface functionalization by metal nanoparticles can be mentioned [14]. It is important to note that the resolution of strain measured is directly related to the geometry of the pattern used and the grating pitch. It appears that specific surface functionalization have to be used for local strain characterizations at the surface of polymeric materials.

Different methods are used to deposit speckle patterns on the surface of polymeric specimens. Paint, black crafting glitter dispersion on a white base coating and spraying are often used [15–19]. In the case of paint, black speckle pattern is sprayed on a base white background. The dimension of the random black speckles are generally in order of millimetre. Recently, for the strain measurements of large 3D printed parts using digital image correlation (DIC), 1 mm black crafting glitter (Horizon Group USA) was randomly applied with a shaker and deposited by gravity on the fresh white paint. A flat white base coating was uniformly applied using Rustoleum Ultra Cover Paint + Primer firstly [16]. With these speckle dimensions, it is difficult to probe kinematic fields at the microscopic and nanometric scales. To better understand the mechanical behaviour of AM polymeric materials at the local scale, the challenge is to access local strain states on the specimens during testing. It is then necessary to develop an approach to deposit appropriate speckles for studies at micro and nanoscales.

Most of these specimen surface preparations are coupled with contactless methods [20]. Digital image correlation is today a mature technique for material property characterizations. The DIC technic consists of comparing two images of the same scene, typically an object under load, and retrieving the displacement field that allows for the best match. In fact, the image is segmented into subsets. The population and dimensions of speckles in each subset play important role in the resolution of the technic. Thanks to its simplicity and accessibility DIC is one of the most used technique for kinematic measurements by converting measured pixel displacement to local strain [21] [22]. DIC has a number of advantages over contact strain measurement methods (e.g. strain gauges or extensometers) including the ability to detect spatially varying strains, adaptability to aggressive environments, and suitability for soft materials such as polymers for which adhesive strain gauges would cause local stiffening and inaccurate strain detection [23].

In this study, an airbrush technique is used to deposit a microscopic speckle on the surface of polymeric specimens obtained by material extrusion. This preparation is coupled to digital image correlation. The local kinematic fields are then followed during an in situ tensile test. The experimental method is used to examine the fracture behaviour of ABS (Acrylonitrile Butadiene Styrene) 3D printed specimens [24]. A previous study was carried out to produce tensile specimens with oriented and classical depositions [25] in order to compare two different mechanical behaviours. The full field strain maps obtained evidence the strain evolutions at filament and interfilament scales during the test. The quantitative analysis of strain maps leads yields fracture toughness determination via J-R curves. In addition, these changes are compared with the macroscopic response of the material. This leads to a better

understanding of structural effect on the mechanical properties and then enhancing these properties by topology optimization.

In the next section, the experimental approach is detailed. The description of the specimen 3D printing settings, polishing, speckle application and experimental device are presented. The microscale kinematic field experimentally measured will be used to study the effect of material structure on the specimen fracture chronology.

## 1. Experimental procedure and methodology

In this section, the details of the sample preparation and the implementation of the test are presented as well as the digital image correlation analysis.

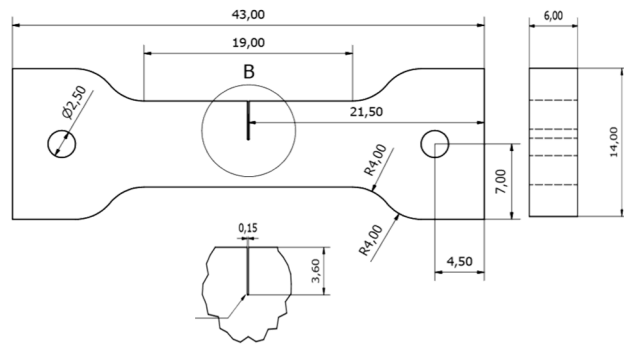
### 1.1. Specimen preparation

A mini SENT specimen is 3D printed with the dimension shown in **figure 1a**. The notch was also made by AM. The notch dimension meet ASTM E1820 and ASTM D6068 standard recommendations, namely,  $a_0/w=0.45$  where  $w$  is the specimen width, and  $a_0$  the initial crack length.

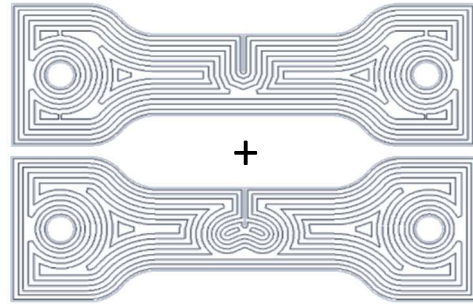
The specimen is printed by adding melted layers of Acrylonitrile butadiene styrene (ABS) using a Makerbot replicator 2X. The specimen is mechanically polished in order to ease the surface functionalization. The initial thickness of the 3D printed specimen was 6 mm and the final thickness after polishing was 3 mm. All samples were printed as solid part, in flat part orientation, build plate temperature was set to 110 °C, the extrusion temperature was 235 °C and layer thickness of 0.25 mm (except for the first layer 0.3 mm).

Depending on deposition trajectory, build orientation, print speed, temperature, and layer width, the mechanical properties of 3D printed parts can be modified [15,17,18]. In the present study, two sample configurations were fabricated. In the first configuration, layers are made by curved filament oriented concentrically around the notch root. This layer deposition method was recently proposed by Gardan et al [25] to improve the fracture toughness of 3D printed parts. Finite Element (FE) simulation of a linear elastic model has been used to compute the principal stress and strains in the samples with plane stresses conditions in order to reproduce both principal directions through deposition trajectories. For this reason, the thickness dimension of the specimens is built by alternate layers. For two subsequent layers, the first principal direction is used to calculate the trajectory in the first layer and so on for the second principal direction and the second layer. Two main orientations of layers are deposited alternatively until the desired thickness is obtained. The sample with this configuration is called “SENT\_oriented” to simplify the nomenclature (see figure 1b).

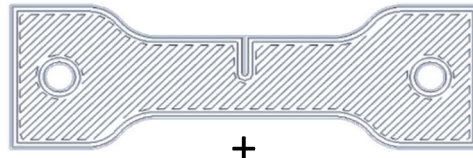
In order to demonstrate the capability of the process developed herein to give precious details at local scales in different material configurations, a totally different configuration was printed in which, layers are made by linear filaments with an angle of +45 and -45 and are alternatively deposited. SENT samples given by this succession of +45° and -45° layers are designated “SENT\_+/-45°” (see figure 1c).



a) SENT sample dimensions (mm)



b) Oriented deposition: even and odd layers



c) +/- 45 ° deposition: +45° and -45° layers

**Figure 1:** Sample geometry and filament orientations

### 1.2. Speckle deposition

In this study, an original speckle pattern with micrometric dimensions is deposited. Contrary to the conventional process of speckle pattern deposition with white base coating, in the present study, the sample surface (red) was used as is. White speckles with micrometric dimensions were deposited using an airbrush [26]. With this technique, it is possible to spray a pattern with dimensions of several millimetres. The analysis of the speckles shows that most of them have their diameter varying between 10  $\mu\text{m}$  and 30  $\mu\text{m}$  with an average diameter of 20  $\mu\text{m}$  (see Figure 2-a)). **Figure 2b shows the autocorrelation of the speckle pattern. The half width of auto-correlation can be used to estimate the radius of speckle [27]. It confirms that speckles average diameter is about 20  $\mu\text{m}$ .**

### 1.3. In situ tensile test

Once the speckle pattern deposited onto the surface of the sample, an in situ tensile test under a digital microscope was conducted. The experimental set up consists of a numerical microscope Keyence VHX-1000 for the surface observation, a tensile micro machine and triggering system (see figure 2-c and table 1). The later allows images to be recorded at specific rates when the specimen is continuously loaded and relate each image to the corresponding applied load.

Table 1. Experimental set-up parameters

Microscope	Keyence VHX-1000
Definition	54 Megapixel 3CCD
Lens	VH-Z100R (100 x to 1000 x)
	Wide-range zoom lens
Field of view	3.05 x 2.28 mm <sup>2</sup>
Working distance	25 mm
Image scale	2 μm/pixel
Image acquisition rate	1 fps
Patterning technique	airbrush
Pattern feature size	10 pixels
Load cell	5kN
Cross-head displacement rate	1.5 μm/s

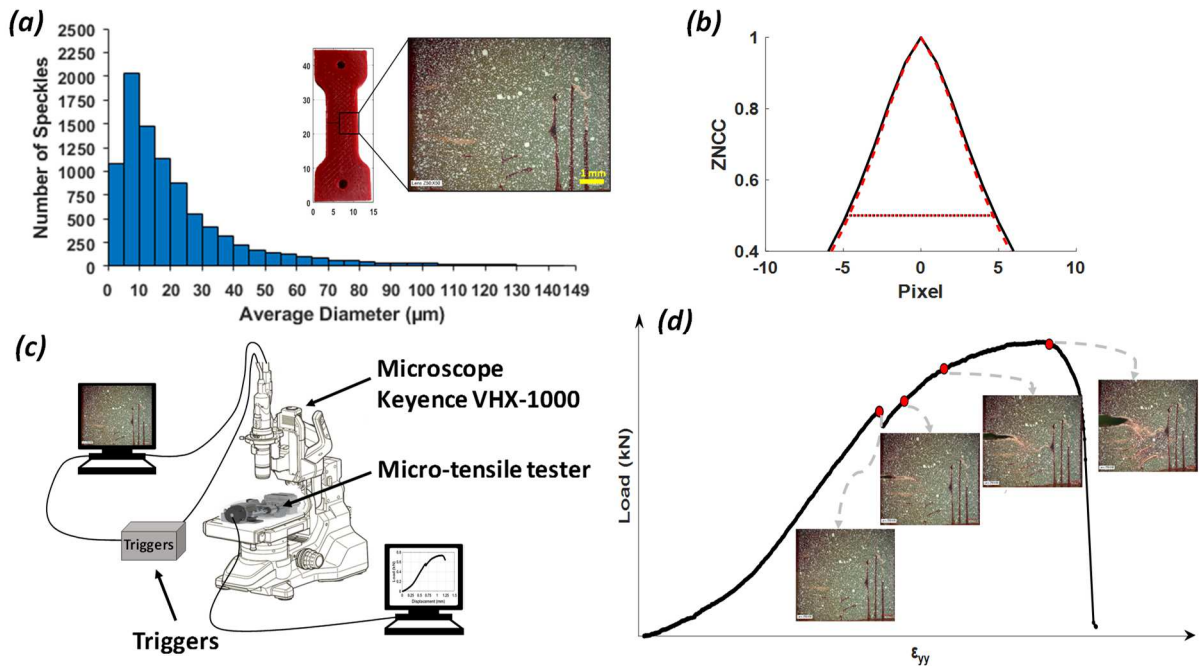


Figure 2: a) Micro speckle pattern and diameter distribution at the sample surface, b) Autocorrelation c) Experimental set up, d) Load-strain curve

## 2. Experimental results

Tensile tests were carried out on mini SENT specimens under a crosshead speed of 1.5 μm/s. Tensile tests were carried out at room temperature on a micromachine with 5 kN loading cell and mounted on the microscope (see **figure 2b**). One image per second was recorded during the test until failure.

### 2.1. Qualitative Analysis

The procedure developed herein makes it possible to obtain, during the test, both local and global data. On the one hand the load-strain curve (macroscopic scale) and on the other hand images evidencing the evolutions of local strains (micro-scale). Each image is associated with specific load and cross-head displacement.

In this section, the results from the specimen printed in the first configuration (SENT-oriented) will be presented. The optical images obtained during the in-situ tensile test allow a

qualitative analysis of the local strains on the material surface. Figure 3 shows the load vs strain curve where  $\epsilon_{yy}$  is the true strain in tensile direction. This curve is associated with some images in order to illustrate the main local features at the specimen surface.

Figure 3 highlights three essential zones. The first zone corresponds to elastic deformations of the material. This linear response is abruptly stopped at step 435 by the load drop which is due to the notch reopening. The notch was welded due the temperature of filament deposition and the dimension of the notch (150  $\mu\text{m}$  of width). The second zone starts with notch blunting until crack initiation. Then a stable propagation zone where plastic deformations develop as the crack is propagating. At the end of this zone, large deformations forming arcs appears (see figure 3, step 719). These shapes are probably due to the filament orientations. At this moment the strain is no longer concentrated only in the crack vicinity but rather in the joints between rasters. This distribution of strains at the interfilament joints increased the capacity of the structure to accommodate the applied load. This is macroscopically evidenced by the plateau in the load – strain curve which start after step 719. The evolution of the plateau and the decreased of the applied load until the failure develops (zone 3). The decrease in load could be linked to the appearance of multiple cracks in welding lines, which ultimately caused global failure. The load drop caused by global failure was progressive because of the one-by-one filament failure shown (see Figure 3; Step 940).

By comparing the tensile curve and the local material surface images in the vicinity of the notch, the experimental method allows for the analysis of the specimen fracture. The effect of the material structure on its toughness is already visible. One can notice that, as shown by images, speckles pattern held up even for large deformations. Therefore, the microscopic kinematic fields obtained by digital image correlation will be relevant even in large deformations.

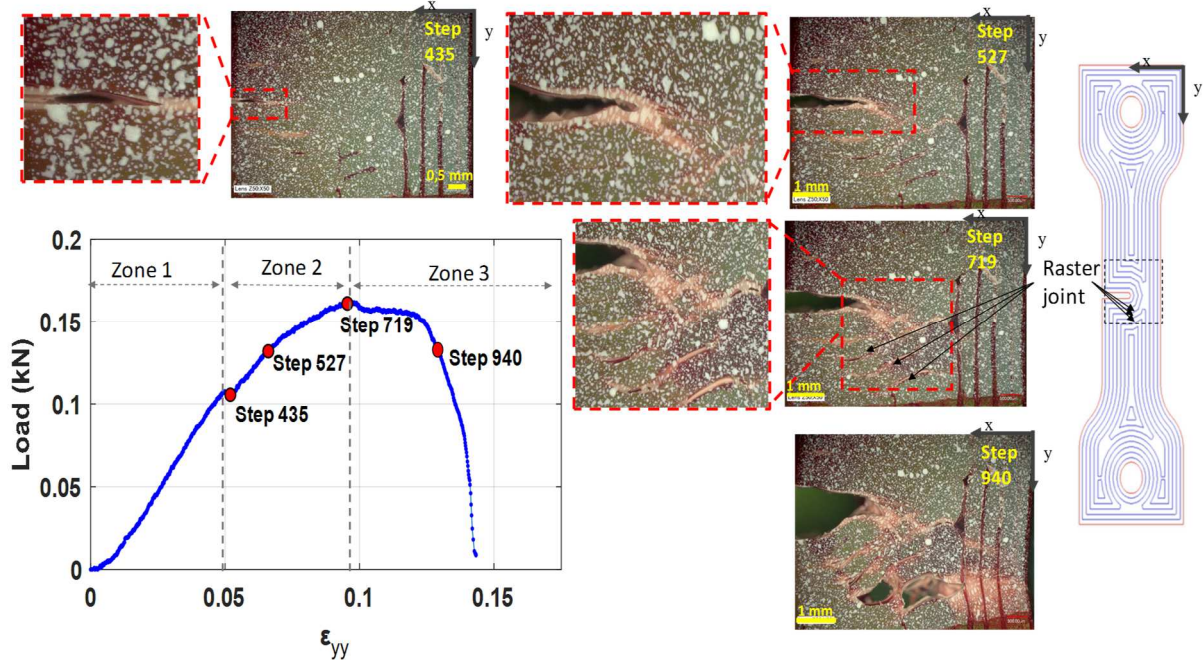


**Figure 3:** Optical analysis of the fracture chronology (oriented deposition)

## 2.2. Quantitative analysis

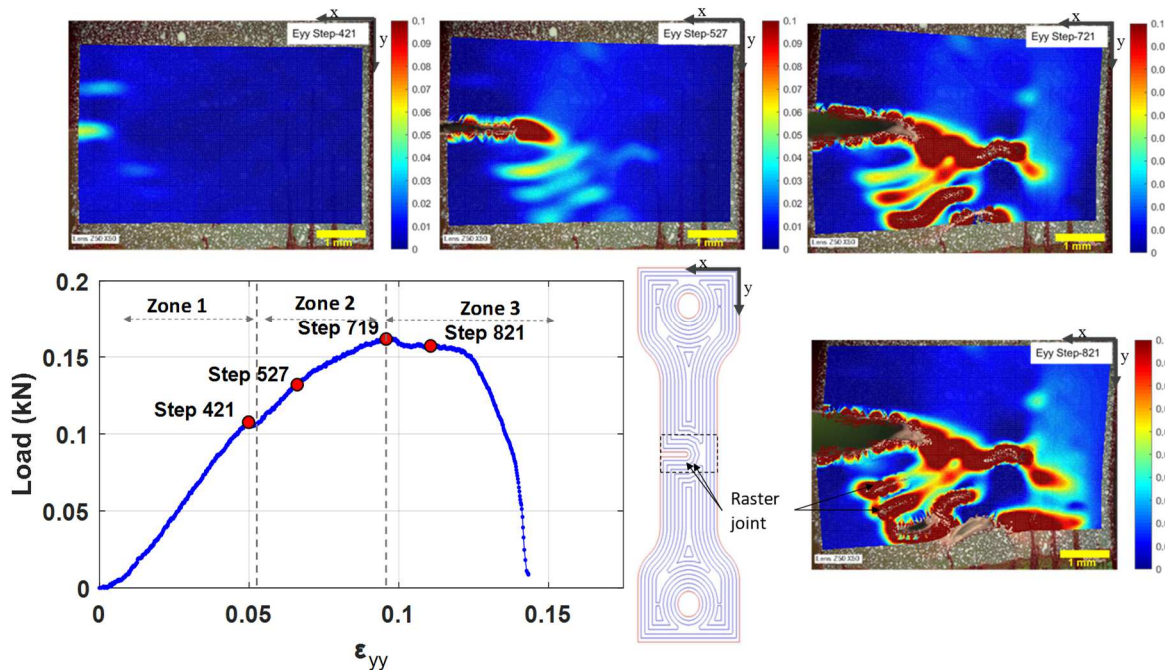
Ncorr [28] software was used for the strain quantitative analysis. Ncorr is an open-source 2D-DIC MATLAB Software developed at Georgia Institute of Technology. Furthermore, this software integrated the modern algorithms of DIC [15]. The software tracked displacement of speckles painted on each image during mechanical loading and used this information to calculate kinematic field maps. In this section, the measured strain field variations are followed. The measurement uncertainty is studied by calculating the scatter of the measured strains values. Table 2 summarize chosen DIC analysis parameters.

Table 2. DIC analysis parameters

DIC software	Ncorr [28]
Subset radius	25
Subset spacing	3
Matching criterion	normalized cross correlation criterion normalized least squares criterion [28]
Strain calculation	2D Savitzky-Golay (SG) digital differentiator [28],[29]
Strain window size	25

### 2.2.1. Strain field analysis

Figure 4 shows longitudinal strain fields obtained by DIC. In zone 1, the strain was uniformly distributed at the material surface. At step 421 strain concentration are visible at the notch position just before reaching step 435 where the notch reopening occurs. In zone 2, although the highest strain concentration is found at the root of the notch, elsewhere strain distributions are non-uniform. Several authors [17,30] reported such phenomena and attributed them to 3D-printed filament configurations. Here, in the case of oriented deposition, the strain concentrated in curved locations corresponding to the filament orientations. These locations are filament welding joints. Stable crack propagation begins and proceeds in the desired direction prescribed by filament orientations.



**Figure 4:** Strain field analysis of fracture events (oriented deposition)

### 2.2.2. The resolution of the method

In order to evaluate the measurement errors attached to the experimental method developed herein, an analysis was conducted focusing on the very beginning of the test. At this stage, it seems like no loading is applied to the sample. Figure 5a shows that the load recorded up to the 55<sup>rd</sup> step is very low and does not exceed 12N, this value can be considered as load measurement uncertainty caused by noise. Beyond step 55 the test piece is loaded in tension. The processing of images recorded at this level **allow the evaluation of uncertainties of kinematic fields**. The displacement measured in tensile direction here named  $v$  is studied by calculating spatial standard deviation  $\sigma_v$  on each step image (see figure 5b). Two zones are determined from the graph of figure 5b, the first one until step 55 where  $\sigma_v$  is equal to  $5 \mu\text{m}$  and it is almost constant (zone 0). Beyond this step the standard deviation increase continuously (zone 1 in figure 5.b). Knowing that in this zone 0 no load is applied to the specimen, it becomes relevant to say that displacements detected here are due to noise and that the measurement uncertainty of the displacement is about  $5 \mu\text{m}$ . The same analysis is carried out on strains obtained in the loading direction  $\epsilon_{yy}$ , figure 5c. Results show that strain standard deviation  $\sigma_{\epsilon_{yy}}$  in the no loading zone (zone 0) is about  $1.3 \cdot 10^{-4}$  which is the strain measurement uncertainty. **From step 55, in addition to the noise the displacements (strains) at the surface of the material can be probe by the developed method.**

Experimental device set up and the image correlation parameters chosen in this study makes it possible to measure displacements and strains with an uncertainty of  $5 \mu\text{m}$  and  $1.3 \cdot 10^{-4}$  respectively for loading level higher than 12N.

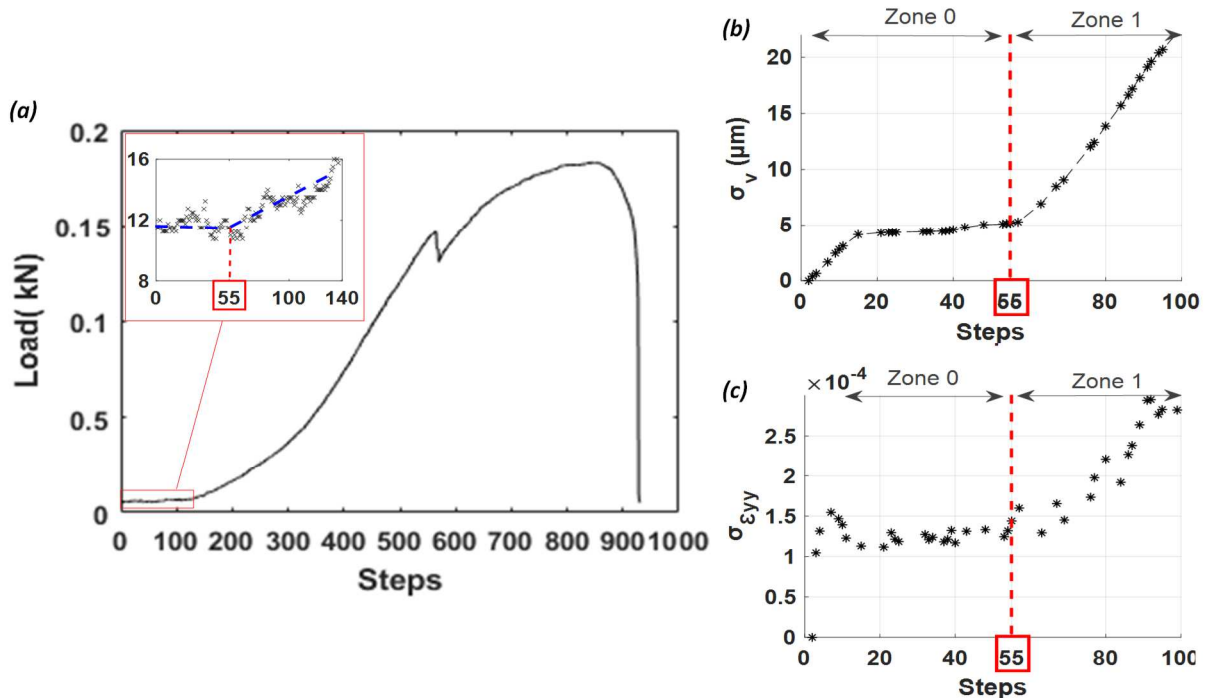


Figure 5: Load, displacement and strain uncertainty

### 3. Fracture mechanics

Fracture mechanics is commonly used to evaluate the toughness of materials. These estimations are no longer based on the failure process of the whole structure, but rather on fields in the crack vicinity. The parameters of linear fracture mechanics (LEFM) such as the Stress Intensity Factor (K) or the energy release rate (G) have limited applicability because of the pronounced plastic behaviour of polymer materials, which causes blunting of the crack tip [31,32]. Originally developed as part of linear and non-linear elasticity, the J integral [33] has been extended to solve the failure problems with plasticity.

The plastic strain which appear before and during failure, confirm the ductile behaviour of the polymeric material obtained with these 3D printing settings. In such material, the resistance to slow stable crack growth after initiation becomes a function of the size and geometry of the specimen [34]. Therefore, it can no longer be represented by a single parameter (Kc or Gc) but rather by a curve ( $J = f(\Delta a)$ ), which takes into account the effect of crack extension  $\Delta a$  as well as the nonlinear behaviour. This curve describes the energy conditions for crack extension.

Testing Procedure to determine the J-R curve of plastics material was established by ASTM D6068 standards [35]. A series of specimens are loaded to different displacements using crosshead or displacement control. The resulting crack fronts are marked, and the crack extensions are measured from the fractured surface. Each displacement step gives a point ( $\Delta a$ , J) on the curve.

Since the experimental method developed in this study allows to follow the growth of the crack, the J-R curve building procedure can be applied efficiently and quickly. The crack extension  $\Delta a$  can be measured through the recorded images during the experiment. The J-integral can be directly calculated as a function of the deformation energy U according to the ASTM D 6068-96 recommendation:

$$J = \frac{\eta U}{b(w - a_0)} \quad (3-1)$$

where  $b$ ,  $w$  and  $a_0$  are, respectively, the specimen thickness, specimen width and the initial crack length,  $U$  the area under the load – displacement curve,  $\eta$  a shape parameter that depends essentially on the ratio  $a_0/w$  [36].

Although the SENT specimens used in this study are not following the ASTM 6068 standard, the method remains valid with  $\eta$  given by [37,38]:

$$\eta = \sqrt{1 + \left(\frac{a_0}{w - a_0}\right)^2} + \frac{a_0}{w - a_0} \quad (3-2)$$

#### 3.1. Identification of the crack tip location

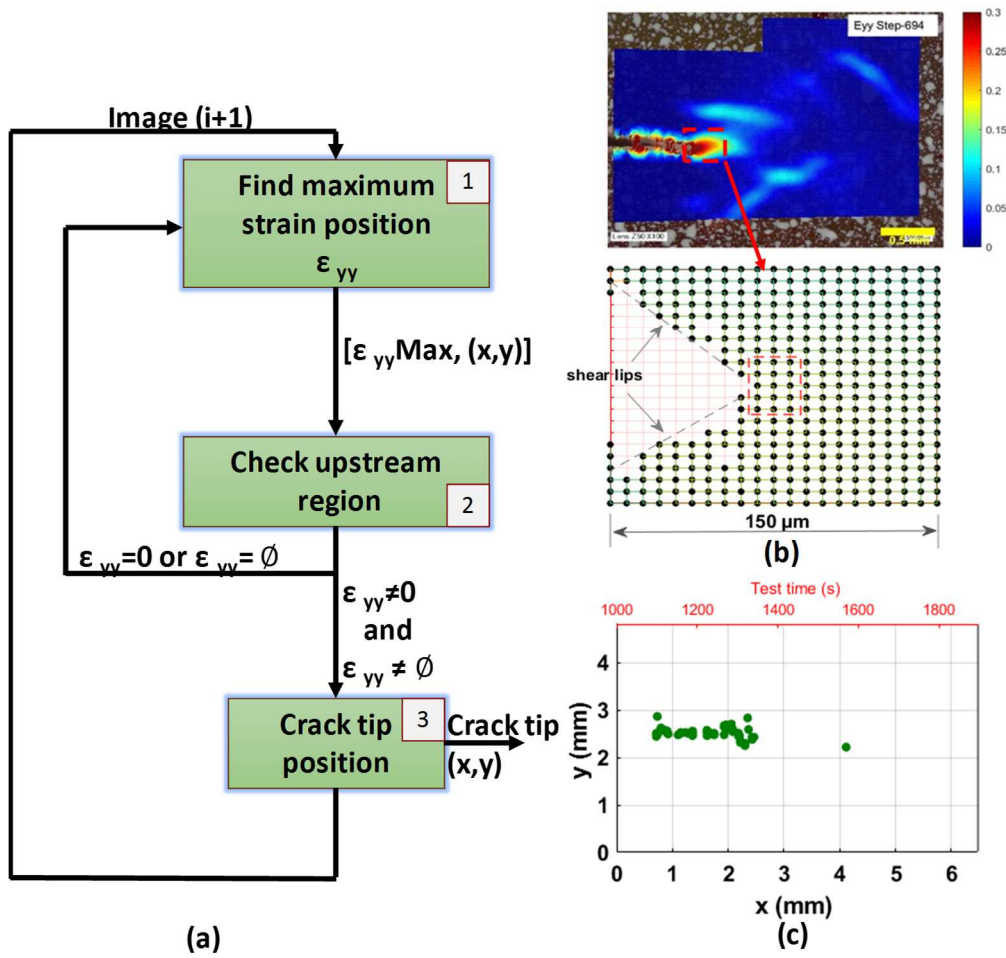
Researchers in the fracture mechanics are confronted to the difficulty of estimating accurately the crack tip location and especially in the case of polymer-based material[37–40]. In such materials large plastic deformation and severe necking at crack tip makes difficult the crack growth measurement[39]. By taking advantages of the experimental parameters of the

specimen surface functionalization; the speckle size, their good adhesion to material surface and DIC efficiency, the crack tip position can be followed automatically during the test.

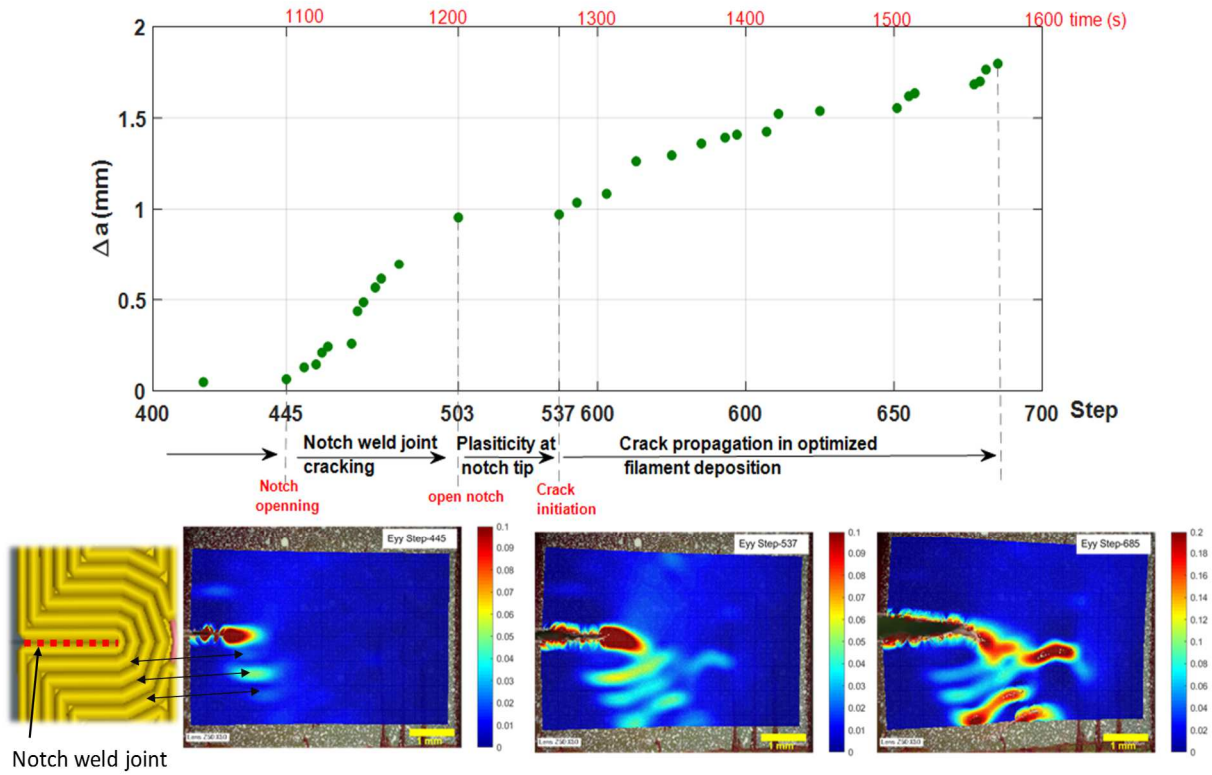
The algorithm developed to identify the crack tip location in the SENT test specimens assumes that, in the crack vicinity, the strain reaches its maximum at the crack tip. So, the crack tip position is found by locating the maximum of the strain values in the loading direction “ $\epsilon_{yy}$ ”. An auxiliary function that identifies discontinuity in the strain field was needed to check if the founded maximum is at the crack tip. This verification is performed on a square region upstream of located point (see figure 6b). The maximum location corresponds to the crack tip only if this region is free of discontinuity (all values are  $\epsilon_{yy} \neq 0$  and  $\epsilon_{yy} \neq \emptyset$ ). The mains steps are shown in figure 6a. Crack initiation and stable growth in SENT specimen during uniaxial loading are obtained by running this algorithm.

Figure 7 shows crack extension as function of steps (image acquisitions) and time. It emerges from this figure similar failure stages than those identified previously until the samples global failure. At the beginning of the test, no crack propagation is noticeable. Once reaching the step 435 ( $t = 1068$  s), the crack initiate and propagate at weld joint between the two filaments forming the edge of the notch. The crack growth rate is about 0.01 mm/s. At step 503 ( $t = 1204$  s) notch is totally open and blunting of takes 68 s (from step 503 to 537). Blunting leads to crack initiation at step 537 ( $t = 1272$  s). Crack propagates by breaking fused filaments and their interface areas with a speed of 6.7  $\mu\text{m/s}$  until step 719 ( $t = 1636$  s). The crack tip position in global failure was not detected because of large strains and non-uniform distributions after step 719.

The methods developed here tracks automatically crack growth on sample surface. The smallest crack growth which can be detected here is about 7.5  $\mu\text{m}$ . This level of measurement is particularly interesting in the case of materials from additive manufacturing because it is less than the filament width (250  $\mu\text{m}$ ).



**Figure 6:** a) Crack tip location algorithm, b) Strain matrix representation (step 609), c) crack tip position in SENT-oriented



**Figure 7:** Fracture chronology based on crack tip displacement and strain field in the crack vicinity (for oriented deposition specimen)

### 3.2. J-R curve construction

The J-R curve for ABS material 3D printed with oriented deposition is obtained by processing the local DIC data as described thereafter. Data were fitted to a power law:

$$J = C_1 \Delta a^{C_2} \quad (3-3)$$

with  $C_1=4.16$  and  $C_2=0.09$ , which met ASTM 6068 Standard recommendation.

Figure 8 shows the curve for the case of the oriented deposition specimen. The J-R curve highlights the very ductile behaviour of the 3D printed ABS material by orienting filament deposition around a notch. This is evidenced by the low value of the exponent  $C_2$ . The present results are consistent with the authors' conclusions when developing this particular material [25,41].

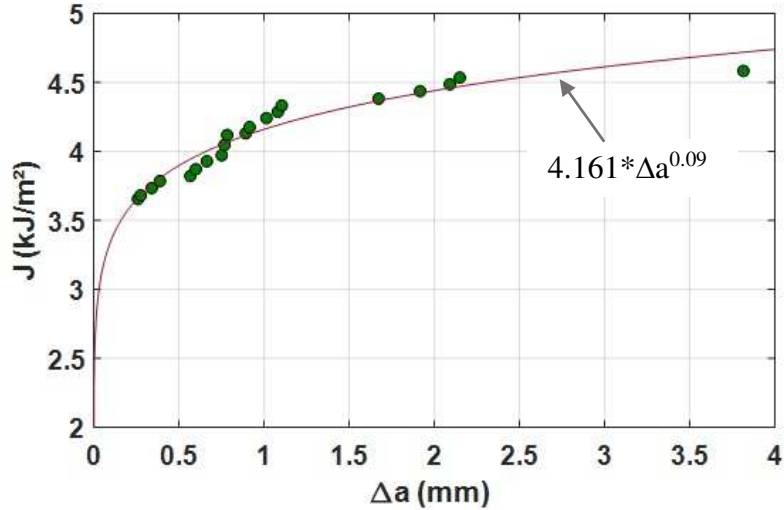


*Figure 8: J-R curve for oriented deposition*

In the next section, this method will be applied to the second configuration (printed with linear filament orientations) in order to test its repeatability and its consistency.

#### **4. Process validation**

##### *4.1. Analysis crack propagation in +/-45 deposition*

Crack initiation and stable growth in the SENT\_+/-45° sample during uniaxial loading are obtained by applying same procedure as before. Figure 9 shows the specimen failure steps. At step 566 a crack initiates and propagates at weld joint between the two filaments forming the edge of the notch. The crack growth rate is the same as for SENT\_oriented (about 10 μm/s). At step 648 (t = 886 s), notch is totally open and blunting takes only 10 seconds (from step 648 to 658). Blunting leads to crack initiation at step 658 (t = 896 s). Crack propagates by breaking rasters and raster's joints with a speed of 6.7μm/s until step 838. The crack follows the junction in the direction at + 45° but this privileged direction is blocked by the filaments oriented -45°. The junction formed by the knot made of two neighbouring weld filaments (raster) oriented + /- 45° are locally strain barriers. The white arrows in the map of the step 838 in figure 9 shows an example of weld filament junction. This structural phenomenon concentrates the strains in the middle plane of the specimen where the final failure occurs.

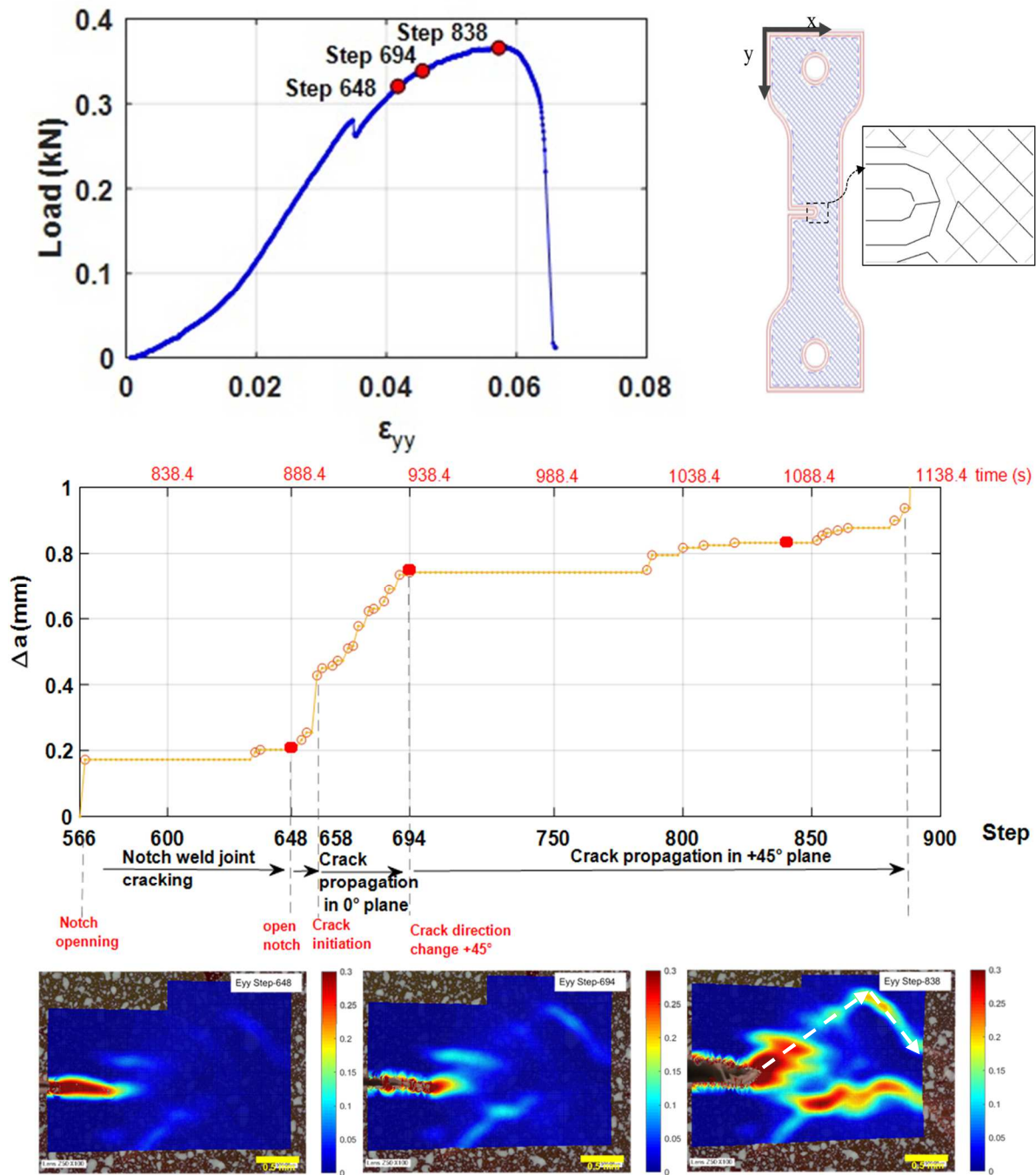


**Figure 9:** Fracture chronology based on crack tip displacement and strain field evolution in the crack vicinity (+/-45° deposition)

#### 4.2. Effect of deposition method on mechanical properties

The J-R curves show that +/-45° deposition has a higher toughness Exponent  $C_2$  increased from 0.09 for oriented deposition to 0.114 for +/-45° deposition. This configuration has a lower ductility since  $\epsilon_{yy}$  at failure is about 0.07 against 0.13 for oriented configuration.

For samples containing +45/-45° raster, the weakest plane can either be above or below the original crack as they are symmetric. By propagating at a 45° angle away from the crack plane (Figure 10.c), it is following the path of least resistance [42]. Strain concentrations are located at filaments joint zones shown by green arrows in figures 10.b. and 10.c. In the oriented

structure (figures 10d and 10e) strain concentrations have a curved shape. This means that the deformation is concentrated at the weld joint between filaments that were deposited with a curved path. This curvature makes the material more ductile.

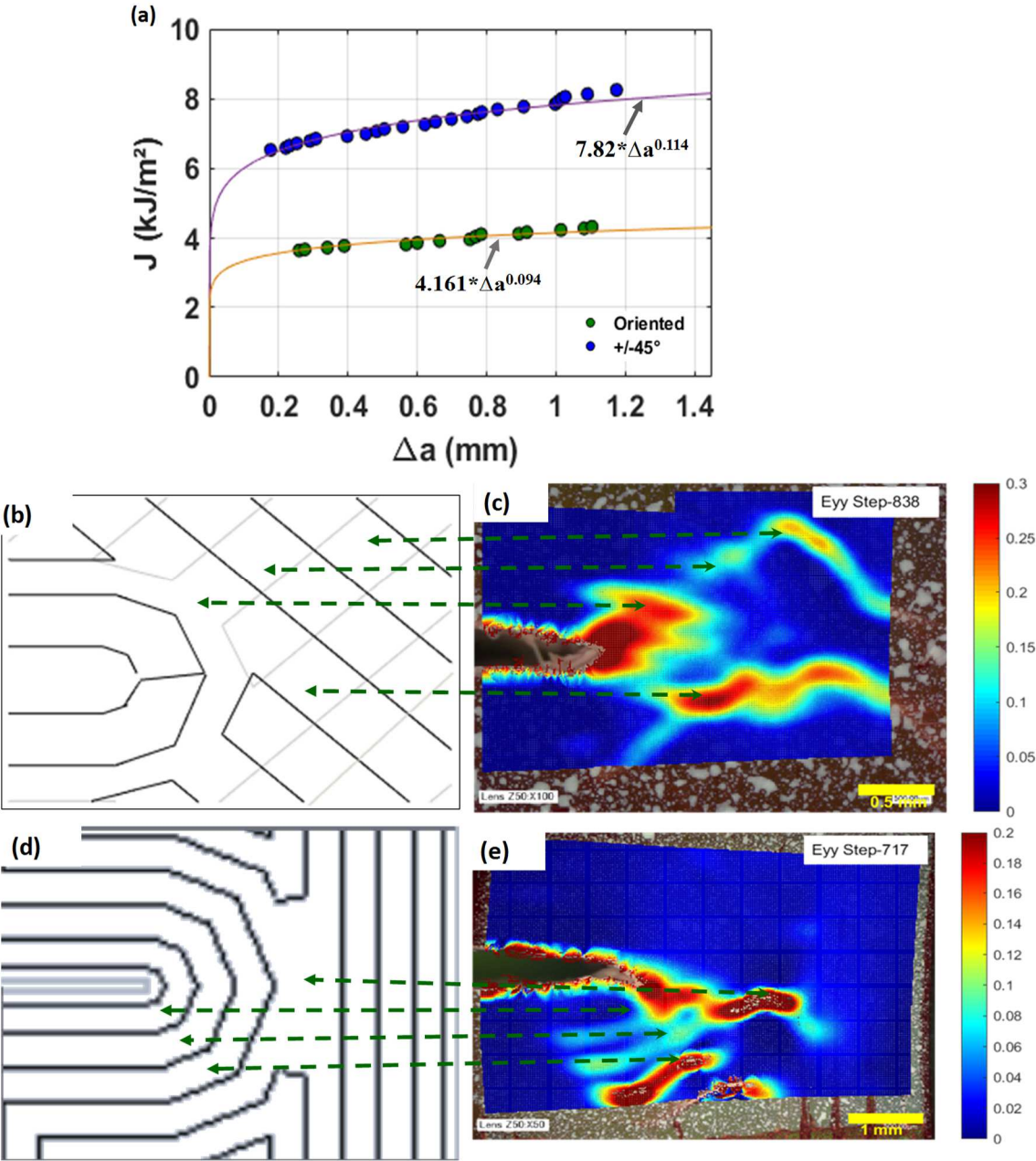


**Figure 10:** Effect of deposition method on material toughness (a) J-R curve (b) +/-45° Structure (c) corresponding strain field, (d) Oriented structure (e) corresponding strain field.

**5. Conclusions**

In this paper, an original and simple experimental method is developed for local strain characterization at the surface of polymeric materials produced by additive manufacturing. The images of the specimen surface acquired during tensile tests associated with load-strain curves allows a qualitative analysis of materials fracture behaviour. The micro speckle pattern deposited onto the surface of the specimen ensures the strain quantification through digital image correlation. Thanks to speckles sizes and high resolution images, refined discretization

has become possible which results in very precise measurement of the kinematic fields at the micrometric scale. These analyses are particularly interesting for understanding the behaviour at the filaments width and the interface area between fused filaments. To take advantage of the method accuracy, crack growth is automatically monitored. Here, the smallest measured crack extension is about  $7.5 \mu\text{m}$ . Then, the material toughness is assessed by means of J-R curves. By comparing the results obtained in both deposition configurations study herein, it appears that  $\pm 45^\circ$  deposition has a better toughness but a lower ductility than the oriented deposition. The strain fields show concentrated zones with curved shape for the oriented deposition, and a linear shape at  $\pm 45^\circ$  following the interface area of fused filaments. These results confirm that the experimental method developed in this study reflects well the effect on material structures on kinematic fields and therefore on the mechanical properties.

The approach developed herein presents great potential for local characterization of materials in general and for polymers specifically because of the limitations they present in regard to classical approaches. It also brings precious details that could help for the optimization of smart materials or structured materials obtained by additive manufacturing.

## Bibliography:

- [1] A. Gebhardt, Understanding Additive Manufacturing, 2011. <https://doi.org/10.3139/9783446431621.fm>.
- [2] J.-P. Kruth, M.C. Leu, T. Nakagawa, Progress in additive manufacturing and rapid prototyping, *CIRP Ann. - Manuf. Technol.* 47 (1998) 525–540. [https://doi.org/10.1016/S0007-8506\(07\)63240-5](https://doi.org/10.1016/S0007-8506(07)63240-5).
- [3] S.A.M. Tofail, E.P. Koumoulos, A. Bandyopadhyay, S. Bose, L. O'Donoghue, C. Charitidis, Additive manufacturing: scientific and technological challenges, market uptake and opportunities, *Mater. Today*. 21 (2018) 22–37. <https://doi.org/10.1016/j.mattod.2017.07.001>.
- [4] J. Gardan, Additive manufacturing technologies: State of the art and trends, *Int. J. Prod. Res.* 7543 (2015) 149–168. <https://doi.org/10.1201/9781315119106>.
- [5] S.H. Ahn, M. Montero, D. Odell, S. Roundy, P.K. Wright, Anisotropic material properties of fused deposition modeling ABS, 2002. <https://doi.org/10.1108/13552540210441166>.
- [6] D. Prall, R.S. Lakes, chiral honeycombe. Poisson's ratio. 1. INTRODUCTION Cellular solids are used widely in a variety of engineering applications. In particular, *Int. J. Mech. Sci.* 39 (1997).
- [7] J. Marae-Djouda, A. Gontier, R. Caputo, G. Lévêque, B. Bercu, Y. Madi, G. Montay, P.-M. Adam, M. Molinari, S. Stagon, T. Maurer, Dense Brushes of Tilted Metallic Nanorods Grown onto Stretchable Substrates for Optical Strain Sensing, *ACS Appl. Nano Mater.* 1 (2018) 2347–2355. <https://doi.org/10.1021/acsanm.8b00441>.
- [8] T. Maurer, J. Marae-Djouda, U. Cataldi, A. Gontier, G. Montay, Y. Madi, B. Panicaud, D. Macias, P.M. Adam, G. Lévêque, T. Bürgi, R. Caputo, The beginnings of plasmomechanics: towards plasmonic strain sensors, *Front. Mater. Sci.* 9 (2015) 170–177. <https://doi.org/10.1007/s11706-015-0290-z>.
- [9] S.-H. Joo, J.K. Lee, J.-M. Koo, S. Lee, D.-W. Suh, H.S. Kim, Method for measuring nanoscale local strain in a dual phase steel using digital image correlation with nanodot patterns, *Scr. Mater.* 68 (2013) 245–248. <https://doi.org/10.1016/j.scriptamat.2012.10.025>.
- [10] L. Allais, M. Bornert, T. Bretheau, D. Caldemaison, Experimental characterization of the local strain field in a heterogeneous elastoplastic material, *Acta Metall. Mater.* 42 (1994) 3865–3880. [https://doi.org/10.1016/0956-7151\(94\)90452-9](https://doi.org/10.1016/0956-7151(94)90452-9).
- [11] J. Marae Djouda, G. Montay, B. Panicaud, J. Béal, Y. Madi, T. Maurer, Nanogauges gratings for strain determination at nanoscale, *Mech. Mater.* 114 (2017). <https://doi.org/10.1016/j.mechmat.2017.08.014>.
- [12] J. Marae Djouda, Y. Madi, F. Gaslain, J. Beal, J. Crépin, G. Montay, L. Le Joncour, N. Recho, B. Panicaud, T. Maurer, Investigation of Nanoscale Strains at the Austenitic stainless steel 316L surface: Coupling between Nanogauges Gratings and EBSD Technique during in situ Tensile Test ., *Mater. Sci. Eng. A.* 740–741 (2018) 316. <https://doi.org/10.1016/j.msea.2018.10.059>.
- [13] J. Marae Djouda, B. Panicaud, F. Gaslain, J. Beal, Y. Madi, G. Montay, L. Le Joncour, J. Gardan, N. Recho, J. Crépin, T. Maurer, Local microstructural characterization of an aged UR45N rolled steel: Application of the nanogauges grating coupled EBSD technique, *Mater. Sci. Eng. A.* 759 (2019) 537–551. <https://doi.org/10.1016/j.msea.2019.05.059>.
- [14] J.-F. Lemineur, S. Schuermans, J. Marae-Djouda, T. Maurer, A.M. Ritcey, Size-Modulation of Plasmonic Nanorings Obtained by the Self-Assembly of Gold Nanoparticles and Block Copolymers, *J. Phys. Chem. C.* 120 (2016).

- <https://doi.org/10.1021/acs.jpcc.6b01689>.
- [15] H. Rezayat, W. Zhao, A. Siriruk, D. Penumadu, S.S. Babu, Structure – mechanical property relationship in fused deposition modelling, 000 (2015) 1–9. <https://doi.org/10.1179/1743284715Y.0000000010>.
- [16] K. Schnittker, E. Arrieta, X. Jimenez, D. Espalin, R.B. Wicker, D.A. Roberson, E. Paso, U. States, Integrating digital image correlation in mechanical testing for the materials characterization of big area additive manufacturing feedstock, *Addit. Manuf.* 26 (2019) 129–137. <https://doi.org/10.1016/j.addma.2018.12.016>.
- [17] J.T. Cantrell, S. Rohde, D. Damiani, R. Gurnani, L. DiSandro, J. Anton, A. Young, A. Jerez, D. Steinbach, C. Kroese, P.G. Ifju, Experimental characterization of the mechanical properties of 3D-printed ABS and polycarbonate parts, *Rapid Prototyp. J.* 23 (2017) 811–824. <https://doi.org/10.1108/RPJ-03-2016-0042>.
- [18] R.J. Zaldivar, D.B. Witkin, T. McLouth, D.N. Patel, K. Schmitt, J.P. Nokes, Influence of Processing and Orientation Print Effects on the Mechanical and Thermal Behavior of 3D-Printed ULTEM® 9085 Material, (2016). <https://doi.org/10.1016/j.addma.2016.11.007>.
- [19] J. Gardan, A. Makke, N. Recho, Improving the fracture toughness of 3D printed thermoplastic polymers by fused deposition modeling, *Int. J. Fract.* 210 (2018) 1–15. <https://doi.org/10.1007/s10704-017-0257-4>.
- [20] M. Grédiac, F. Sur, B. Blaysat, The Grid Method for In-plane Displacement and Strain Measurement: A Review and Analysis, *Strain.* 52 (2016) 205–243. <https://doi.org/10.1111/str.12182>.
- [21] A.C. Abbott, G.P. Tandon, R.L. Bradford, H. Koerner, J.W. Baur, Process-structure-property effects on ABS bond strength in fused filament fabrication, *Addit. Manuf.* 19 (2018) 29–38. <https://doi.org/10.1016/j.addma.2017.11.002>.
- [22] B. Pan, K. Qian, H. Xie, A. Asundi, Two-dimensional digital image correlation for in-plane displacement and strain measurement: A review, *Meas. Sci. Technol.* 20 (2009). <https://doi.org/10.1088/0957-0233/20/6/062001>.
- [23] F. Hild, S. Roux, Digital image correlation: From displacement measurement to identification of elastic properties - A review, *Strain.* 42 (2006) 69–80. <https://doi.org/10.1111/j.1475-1305.2006.00258.x>.
- [24] J. Gardan, Smart materials in additive manufacturing: state of the art and trends, *Virtual Phys. Prototyp.* 14 (2019) 1–18. <https://doi.org/10.1080/17452759.2018.1518016>.
- [25] J. Gardan, A. Makke, N. Recho, A Method to Improve the Fracture Toughness Using 3D Printing by Extrusion Deposition, *Procedia Struct. Integr.* 2 (2016) 144–151. <https://doi.org/10.1016/j.prostr.2016.06.019>.
- [26] J.M. Djouda, D. Gallitelli, M. Zouaoui, A. Makke, J. Gardan, N. Recho, J. Crépin, Local scale fracture characterization of an advanced structured material manufactured by fused deposition modeling in 3D printing, *Frat. Ed Integrita Strutt.* 14 (2020) 534–540. <https://doi.org/10.3221/IGF-ESIS.51.40>.
- [27] M. Bornert, F. Brémand, P. Doumalin, J.C. Dupré, M. Fazzini, M. Grédiac, F. Hild, S. Mistou, J. Molimard, J.J. Orteu, L. Robert, Y. Surrel, P. Vacher, B. Wattrisse, Assessment of digital image correlation measurement errors: Methodology and results, *Exp. Mech.* 49 (2009) 353–370. <https://doi.org/10.1007/s11340-008-9204-7>.
- [28] J. Blaber, B. Adair, A. Antoniou, Ncorr: Open-Source 2D Digital Image Correlation Matlab Software, *Exp. Mech.* 55 (2015) 1105–1122. <https://doi.org/10.1007/s11340-015-0009-1>.
- [29] B. Pan, Full-field strain measurement using a two-dimensional Savitzky-Golay digital differentiator in digital image correlation, *Opt. Eng.* 46 (2007) 033601.

- <https://doi.org/10.1117/1.2714926>.
- [30] T. Webbe Kerekes, H. Lim, W.Y. Joe, G.J. Yun, Characterization of process–deformation/damage property relationship of fused deposition modeling (FDM) 3D-printed specimens, *Addit. Manuf.* 25 (2019) 532–544. <https://doi.org/10.1016/j.addma.2018.11.008>.
- [31] B. Cotterell, J.K. Reddel, The essential work of plane stress ductile fracture, *Int. J. Fract.* 13 (1977) 267–277. <https://doi.org/10.1007/BF00040143>.
- [32] Y.-W. Mai, P. Powell, Essential work of fracture and j-integral measurements for ductile polymers, *J. Polym. Sci. Part B Polym. Phys.* 29 (1991) 785–793. <https://doi.org/10.1002/polb.1991.090290702>.
- [33] J.R. Rice, A Path Independent Integral and the Approximate Analysis of Strain Concentration by Notches and Cracks, *J. Appl. Mech.* 35 (1968) 379. <https://doi.org/10.1115/1.3601206>.
- [34] X.-K. Zhu, J.A. Joyce, Review of fracture toughness (G, K, J, CTOD, CTOA) testing and standardization, *Eng. Fract. Mech.* 85 (2012) 1–46. <https://doi.org/10.1016/J.ENGFRACTMECH.2012.02.001>.
- [35] ASTM, Standard Test Method for Determining J-R Curves of Plastic Materials, *ASTM Stand. Test Method.* i (2013) 1–8. <https://doi.org/10.1520/D6068-10.2>.
- [36] V. Brosa, C. Bernal, P. Frontini, Calibration of fracture mechanics parameters and J–R curve determination in polyethylene side-grooved arc-shaped specimens, *Eng. Fract. Mech.* (1999).
- [37] R. Taktak, N. Guermazi, J. Derbeli, N. Haddar, Effect of hygrothermal aging on the mechanical properties and ductile fracture of polyamide 6: Experimental and numerical approaches, *Eng. Fract. Mech.* 148 (2015) 122–133. <https://doi.org/10.1016/j.engfracmech.2015.09.001>.
- [38] B. Mouhmid, A. Imad, N. Benseddiq, D. Lecompte, An experimental analysis of fracture mechanisms of short glass fibre reinforced polyamide 6,6 (SGFR-PA66), *Compos. Sci. Technol.* 69 (2009) 2521–2526. <https://doi.org/10.1016/j.compscitech.2009.07.003>.
- [39] M. Elmequenni, M. Naït-Abdelaziz, F. Zaïri, J.M. Gloaguen, Fracture characterization of high-density polyethylene pipe materials using the  $J$ -integral and the essential work of fracture, *Int. J. Fract.* 183 (2013) 119–133. <https://doi.org/10.1007/s10704-013-9848-x>.
- [40] N. Matsumoto, J.A. Nairn, The fracture toughness of medium density fiberboard (MDF) including the effects of fiber bridging and crack-plane interference, *Eng. Fract. Mech.* (2009). <https://doi.org/10.1016/j.engfracmech.2009.04.007>.
- [41] P. Lanzillotti, J. Gardan, A. Makke, N. Recho, Enhancement of fracture toughness under mixed mode loading of ABS specimens produced by 3D printing, *Rapid Prototyp. J.* 25 (2019) 679–689. <https://doi.org/10.1108/RPJ-09-2018-0247>.
- [42] T.D. McLouth, J. V. Severino, P.M. Adams, D.N. Patel, R.J. Zaldivar, The impact of print orientation and raster pattern on fracture toughness in additively manufactured ABS, *Addit. Manuf.* 18 (2017) 103–109. <https://doi.org/10.1016/j.addma.2017.09.003>.